



HAL
open science

Final-state-resolved mutual neutralization in $I^+ - I^-$ collisions

Mathias Poline, Xiang Yuan, Sylvain Badin, Mingchao Ji, Stefan Rosén, Suvasthika Indrajith, Richard D Thomas, Henning Schmidt, Henning Zettergren, André Severo Pereira Gomes, et al.

► **To cite this version:**

Mathias Poline, Xiang Yuan, Sylvain Badin, Mingchao Ji, Stefan Rosén, et al.. Final-state-resolved mutual neutralization in $I^+ - I^-$ collisions. *Physical Review A*, 2022. hal-03768879v2

HAL Id: hal-03768879

<https://hal.sorbonne-universite.fr/hal-03768879v2>

Submitted on 5 Sep 2022 (v2), last revised 16 Nov 2022 (v3)

HAL is a multi-disciplinary open access archive for the deposit and dissemination of scientific research documents, whether they are published or not. The documents may come from teaching and research institutions in France or abroad, or from public or private research centers.

L'archive ouverte pluridisciplinaire **HAL**, est destinée au dépôt et à la diffusion de documents scientifiques de niveau recherche, publiés ou non, émanant des établissements d'enseignement et de recherche français ou étrangers, des laboratoires publics ou privés.

Final-state-resolved mutual neutralization in I^+ - I^- collisions

Mathias Poline,¹ Xiang Yuan,^{2,3} Sylvain Badin,^{2,4} MingChao Ji,¹ Stefan Rosén,¹
Suvasthika Indrajith,¹ Richard D. Thomas,¹ Henning T. Schmidt,¹
Henning Zettergren,¹ Andre Severo Pereira Gomes,² and Nicolas Sisourat⁴

¹*Department of Physics, Stockholm University, Stockholm, Sweden*

²*Université de Lille, CNRS, UMR 8523 - PhLAM - Physique des Lasers, Atomes et Molécules, F-59000 Lille, France*

³*Department of Chemistry and Pharmaceutical Science,
Faculty of Science, Vrije Universiteit Amsterdam,
de Boelelaan 1083, 1081 HV Amsterdam, The Netherlands.*

⁴*Sorbonne Université, CNRS, Laboratoire de Chimie Physique Matière et Rayonnement, UMR 7614, F-75005 Paris, France*

(Dated: today)

We have studied the mutual neutralization reaction of atomic iodine ions (i.e. $I^+ + I^- \rightarrow I + I$) in a cryogenic double electrostatic storage ring apparatus. Our results shows that the reaction forms iodine atoms either in the ground state configuration ($\sim 40\%$) or with one atom in an electronically excited state ($I(6s^2[2])$, $\sim 60\%$), with no significant variation over the branching ratios in the studied collision energy range (0.1-0.8 eV). We estimate the total charge transfer cross section to be of the order of 10^{-13} cm² at 0.1 eV collision energy. *Ab initio* relativistic electronic structure calculations of the potential energy curves of I_2 , suggest that the reactions takes place at short internuclear distances. The results are discussed in view of their importance for applications in electric thrusters.

I. INTRODUCTION

Electric thrusters for space vehicles have been developed across the world since the 1960s. Since then, they have been deployed on hundreds of satellites and space exploration probes [1, 2]. Thanks to the recent increase in available power on spacecraft [1], the full potential of electric propulsion is now achievable. This is demonstrated by the emergence of all-electric communication satellites and projects requiring the deployment of large constellations of small electric-powered satellites [1–3] (see also [4] and references therein).

The basic physical principles of electric thrusters are the following: a plasma is formed by ionizing the propellant, and the ions created are accelerated by electromagnetic fields. The ejection of the accelerated ions produces a thrust to the spacecraft through the conservation of momentum. The efficiency of these systems depends strongly on the total ion density formed in the plasma. An efficient propellant should therefore have high atomic mass and be easy to ionize, in order to yield high ion fluxes and exert a large force on the spacecraft. Xenon is currently the propellant of choice (see e.g. [5] and references therein), owing to its high atomic mass and fairly low ionization potential. However, xenon is rare, expensive, and must be stored either in high-pressure tanks or at cryogenic temperatures, significantly impacting the useable volume in satellites.

The iodine molecule is an interesting candidate to replace xenon [6–9] since it also has high atomic mass and low ionization potential. In contrast to xenon, iodine is cheap and exists in the solid state at standard pressure and temperature. These properties result in a storage density of iodine that is three times higher than that of xenon under equivalent conditions. In an iodine plasma thruster, the electric energy is used to ionize the iodine

molecules to form the plasma. In addition to this ionization, some energy is also inevitably dissipated in other processes, leading to various atomic and molecular iodine species, both neutral and charged. Only ions can be accelerated electrically to participate in the propulsion. However, various reactions taking place in the volume of the plasma can lead to the neutralization of the species, thus causing substantial power loss. There is currently no data available on these processes, thus impeding the description and modeling of such thrusters.

As a first step to address these issues, we have studied a key reaction in iodine plasmas [10], the mutual neutralization (MN) reaction of atomic iodine ions:



where E_K is the kinetic energy released in the process. Recent modeling suggests that this reaction is of importance to the performance of thrusters [10]. However, the model relies on input from experimental studies that are associated with large uncertainties regarding the actual MN collision partners and the related rates in iodine plasmas [11]. Furthermore, the atoms formed in MN collisions can undergo further reactions [6], which rates may depend strongly on the final states of the reaction products. The present study is therefore needed to improve the modeling of iodine plasma.

In MN reactions, the kinetic energy released E_K , is related to the initial- and final-state distributions of the atoms. By measuring E_K , the branching ratios for the different channels in this reaction were determined at the collision energies of ~ 0.1 eV and ~ 0.8 eV. Our results show that i) the reaction leads to two different sets of product pairs: either a pair of atoms in the ground state configuration, or a pair in which one atom is in its ground state while the other is in the $6s^2[2]$ excited state; ii)

these pairs have a population of roughly 40%/60% with no significant dependence on the collision energy in the studied range; and iii) the total charge transfer cross section is of the order of 10^{-13} cm² at 0.1 eV collision energy. Furthermore, insights into the electron dynamics taking place during the collision are provided by potential energy curves for I₂, which we have calculated by means of multi-reference *ab initio* relativistic electronic structure methods. These suggest that the relevant curve crossings leading to the observed final states occur at short internuclear distances.

The outline of the article is the following: in section II, we briefly describe the theoretical and experimental methods employed to study the mutual neutralization reactions of iodine ions. In section III, the *ab initio* potential energy curves of I₂ are discussed and the experimental branching ratios for the different channels in this reaction are reported. The article ends with a summary of this work (section IV).

II. METHODS

A. Theory

The *ab initio* calculations of the electronic states of I₂ were performed with the DIRAC19 release [12] and with a development version (hash 1e798e5) of the DIRAC relativistic electronic structure package[13]. In all calculations we employed the 4-component Dirac-Coulomb (DC) Hamiltonian, which accounts for scalar and spin-orbit effects at the mean-field level. We employed an uncontracted triple-zeta quality basis set, including three diffuse functions (t-aug-dyall.v3z[14]), in order to accurately compute the Rydberg and ion-pair (IPr) states.

The ground and electronically excited states considered here were obtained with the multi-reference configuration interaction (MRCI) method, as implemented in the KRCI module [15] of DIRAC. In the reference configuration for MRCI we employed 10 electrons distributed over 12 spinors. This includes the valence $\sigma_{1/2}, \pi_{1/2}, \pi_{3/2}, \pi_{1/2}^*, \pi_{3/2}^*$ and $\sigma_{1/2}^*$ molecular spinors arising from the p^5 manifold of each atom, and ensures a qualitatively correct dissociation behavior for large internuclear distances. We calculated 109 single point energies within the range of 1.9-10 Å for the potential energy curves (PECs) and sixty-three molecular states in total, for the $\Omega = 0_g, 0_u, 1_g, 1_u, 2_g$ and 2_u symmetries. Spectroscopic constants for the different (bound) electronic states have been derived from the calculated PECs with the LEVEL [16] program.

As our electronic structure calculations account for spin-orbit coupling from the outset, and we are dealing with systems possessing linear symmetry. Thus, instead of employing the commonly used LS-coupling notation to characterize the symmetry of the molecular electronic states, we label them by the value of the projection of the total electronic angular momentum along the inter-

nuclear axis (Ω). For example, the first $\Omega = 0_g^+$ state corresponds to the $^1\Sigma_g^+$ ground-state (for further details on how the DIRAC code handles the attribution of such quantities see Ref. [13]).

B. Experimental details

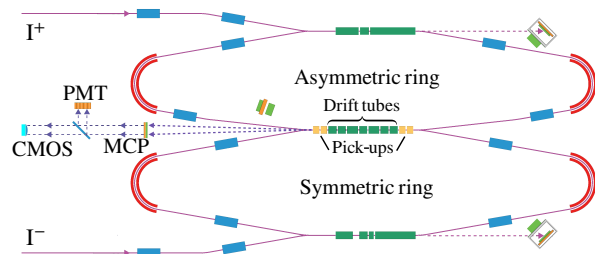


FIG. 1. Schematic of the double electrostatic ion beam storage ring DESIREE. I⁺ and I⁻ ion beams are created from two different ion sources (see text), and injected into the two rings. In the merged section (drift tubes), the ions interact and the resulting neutrals are detected by means of a three-dimensional imaging detector consisting of a micro-channel plate/phosphor screen based detector (MCP), a CMOS camera, and a PMT.

The experiments were carried out at the double electrostatic ion beam storage ring facility DESIREE (Stockholm University, Sweden), an ultra-high vacuum device operated at cryogenic temperatures of about 13 K. This experimental setup has been described previously in Thomas *et al.*[17] (design and technical description), Schmidt *et al.*[18] (first commissioning) and Eklund *et al.*[19] (first mutual neutralization experiment) and is only briefly discussed here.

Positive iodine ions were produced from pure iodine in an electron cyclotron resonance (ECR) ion source and negative iodine ions were produced from magnesium iodide compounds in a cesium sputtering (SNICS) source. Bending magnets at the exit of the sources were employed to select the ions of interest, after which the two oppositely charged ion beams of ¹²⁷I were accelerated and injected into the two storage rings.

As shown in Fig. 1, the two rings share a common section in which interactions between the two species may occur. Pick-up electrodes, located at the entrance and exit of this merged section, measure the beam positions and were used to optimize the overlap of the two ion beams. The collision energy $E_{c.m.}$ of the reaction was then fine tuned through the biasing of drift tubes. This applied voltage decelerates/accelerates the negative/positive ions to the desired velocities in a small section of this merged region (the biased region), allowing to constrain the region of low collision energy interactions (here chosen to be approximately 16 cm long).

A microchannel-plate (MCP) detector[20] located at 1.5m from this biased region was used to detect the

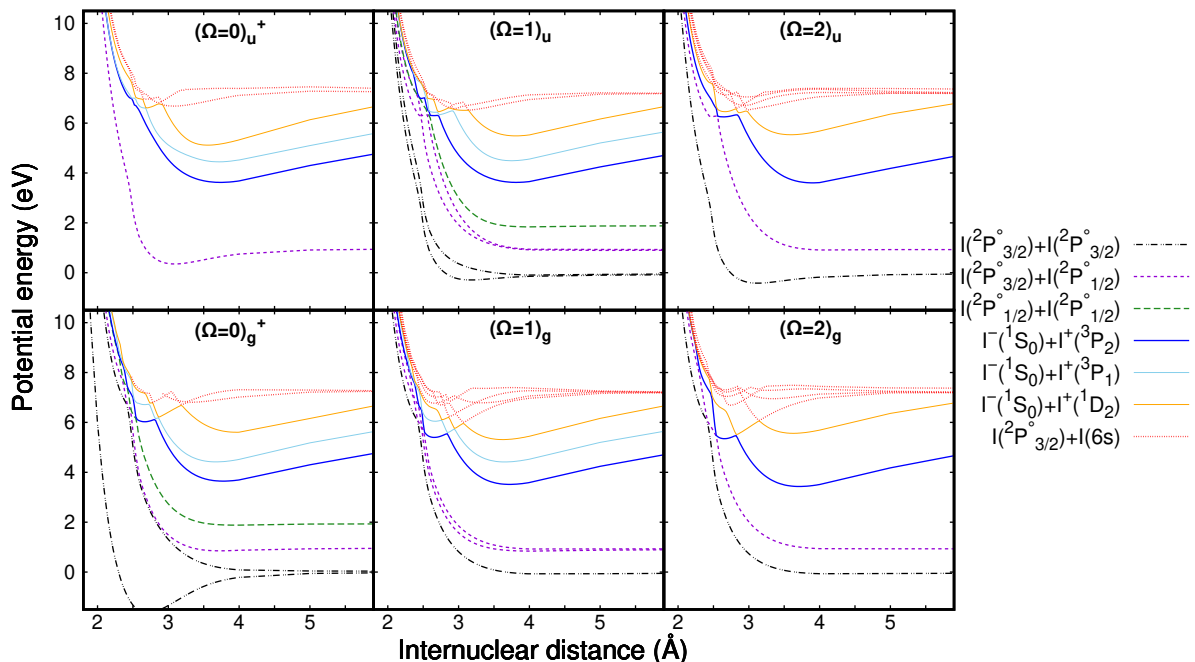


FIG. 2. MRCI PECs of 51 electronic states (including Rydberg and IPR) of I_2 , classified in terms of projection of the total electronic angular momentum Ω . 12 $(\Omega = 0)^-_g$ and $(\Omega = 0)^-_u$ states are not shown here since there is no $I^+(^3P_2) + I^-(^1S_0)$ state with this symmetry. The energies (in eV) have been scaled so that the zero corresponds to twice the energy of the $^2P_{3/2}$ ground state of the isolated iodine atom. See Table III for the energies of the different asymptotes. **Detailed views of the PECs at short internuclear distances are shown in Fig. 6 in the appendix.**

neutralized particles arising from mutual neutralization events and residual gas collisions. Each of these events produced light spots on a phosphor screen located behind the MCP. The resulting photons are guided via optics to a complementary metal oxide semiconductor (CMOS) camera and a multi-anode photomultiplier tube (PMT), which record the positions and relative arrival times of the particles. **This PMT system can detect events with an arrival time difference up to 200 ns. In the unbiased region of the merged section, the relative velocity of the two ions is such that the arrival time differences are well outside this time window. Thus, these events do not interfere with the data from reactions occurring in the biased region.**

C. Branching ratios calculations

For an MN event occurring at a distance L from the detector, the separation between two neutral particles formed in the reaction, as recorded by the detection system, is given by

$$r = \sqrt{r_{\parallel}^2 + r_{\perp}^2} \approx \sqrt{\frac{2(E_K + E_{c.m.})}{\mu}} \frac{L}{v} \quad (2)$$

where r_{\parallel} is the projected transverse distance, recorded by the camera, $r_{\perp} \approx v\Delta t$ an approximation of the third

dimensional component (v being the average velocity of the reactants), and μ the reduced mass of the ions. Here, $E_{c.m.}$ is the center-of-mass kinetic energy before the interaction and E_K is the kinetic energy released in the specific reaction channel.

This particular three-dimensional imaging technique of two particles was first introduced by Z. Amitay and D. Zajfman[21] for the study of the dissociative recombination reaction[22–24] but has since then been employed for a number of MN systems, such as Li^+/D^- [19, 25], Mg^+/D^- [26], and O^+/O^- [27, 28]. The resulting spectrum represents a distribution of the final-state center-of-mass kinetic energy, over the longitudinal extension of the interaction region and the collision energy spread. By simulating these distributions **using the Monte Carlo method** and fitting these to the data, the branching ratios can be extracted[19, 29]. These are corrected for the energy dependent efficiency related to the angular acceptance of the detectors (for more details see reference [28]).

Table 1 shows the experimental parameters used during the three experimental runs: In the first run, data were acquired using slower ion beams in order to investigate the low kinetic energy release (E_K) channels in detail; in the two other runs, data were acquired with the aim of measuring the final state distributions of all energetically open channels at two different collision energies.

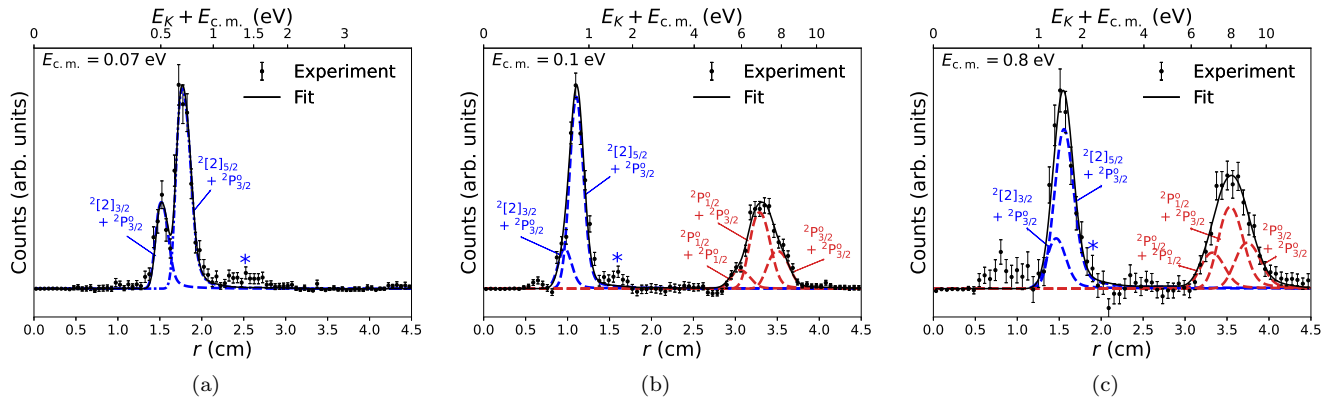


FIG. 3. Yield of neutral pairs as a function of the separation r between the products at center-of-mass collision energies 0.07 eV (a), 0.1 eV (b) and 0.8 eV (c). The top scale shows the corresponding center-of-mass kinetic energy after the reaction (equation 2). The full curve results from a fit of the simulated distributions of ground state/excited state pairs (blue line, equation 3) and ground state configuration pairs (red line, equation 4). The asterisks indicate contributions from metastable cations (not included in the fit). The background has been subtracted (see Figure 5 in the Appendix for original spectra).

TABLE I. Experimental parameters used during the data acquisitions. These show the energies (E_i) and currents (I_i) of the positive (A) and negative (B) ion beam, the potentials applied to the interaction region (U) and the center-of-mass collision energy obtained ($E_{c.m.}$).

Data set	E_A (keV)	E_B (keV)	I_A (nA)	I_B (nA)	U (V)	$E_{c.m.}$ (eV)
1	13	12	3	8	500	0.07 ± 0.01
2	35	30	15	30	1275	0.10 ± 0.02
3	35	30	15	30	1060	0.80 ± 0.10

In order to maximize the range of product kinetic energies that could be detected and obtain satisfying rates, higher beam energies and currents were used in the two later data sets, resulting in larger background contributions. These mainly arise from collisions between stored ions and residual-gas molecules as well as false coincidences. The majority of the background could be filtered out by excluding events for which the center-of-mass position of the two products on the imaging detector were outside a 5 mm range. However, a non-negligible number of events remained after this selection, in particular for measurements with low signal/background ratios. The filtered-out events were then used as a model for this remaining background and subsequently subtracted from the spectra. For more details see Appendix C.

D. Reaction cross section estimate

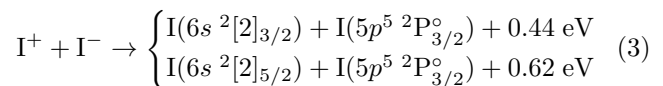
In order to determine MN reaction cross-section, it is necessary to determine the spatial distributions of the interacting particle beams. Currently, a method to derive this overlap (form factor) with high precision is not available at DESIREE. Additionally, it may vary between

different experiments since the storing of merged beams requires adjusting the ion optics based on the mass ratio and energies of the two ions. The cross section may therefore only be roughly estimated based on the observed rates relative to other previously studied systems with known cross sections, and is subject to large uncertainties. However, given the absence of any experimental or theoretical estimate for this particular collision system, we have done such an evaluation, which is presented in the results section.

III. RESULTS AND DISCUSSION

Theoretical results

In order to get insights into the MN dynamics, we report the potential energy curves of I_2 in Figure 2 (a detailed discussion of these curves is given in the appendix). At the collision energies investigated in this work, electronic processes take place mainly around the avoided crossings. Assuming the system starts in the lowest ion-pair state (i.e. $I^+(^3P_2) + I^-(^1S_0)$, blue curve in Fig. 2) one can, in principle, study the paths to a given final state for each symmetry. Since the asymptotic energy of the ion-pair state lies above the excited/ground state pair, the reaction may result in the formation of an electronically excited iodine neutral atom, i.e



As there are too many avoided crossings between the states, an appropriate simulation of the collision dynamics is necessary to study the pathway to these channels. However, the path to the lowest states of I_2 are fairly simple: for all symmetries the lowest ion-pair state exhibits

first an avoided crossing with the curves corresponding to $I(^2P_{3/2}^{\circ}) + I(6s)$ (here shown in red) at an interatomic distance between 2.5 and 3 Å. At shorter interatomic distances, these curves can cross the ground state configuration curves, resulting in the following channels:

$$I^+ + I^- \rightarrow \begin{cases} I(5p^5 \ ^2P_{1/2}^{\circ}) + I(5p^5 \ ^2P_{1/2}^{\circ}) + 5.51 \text{ eV} \\ I(5p^5 \ ^2P_{1/2}^{\circ}) + I(5p^5 \ ^2P_{3/2}^{\circ}) + 6.45 \text{ eV} \\ I(5p^5 \ ^2P_{3/2}^{\circ}) + I(5p^5 \ ^2P_{3/2}^{\circ}) + 7.39 \text{ eV} \end{cases} \quad (4)$$

Therefore, the simplest path to the lowest states of I_2 is through a highly excited state followed by a de-excitation of the excited iodine atom at closer distances between the collision partners.

We note that avoided crossings between the lowest ion-pair state and these excited/ground state pair ones also occur at larger internuclear distances (~ 23 Å). However, using a Landau-Zener approach and the Olson semi-empirical model (see [30], equation 13), we estimate that the electronic couplings at these avoided crossings are negligible. **The dynamics of the reaction are therefore expected to take place at the avoided crossings presented in Fig. 2, for which more advanced modeling is necessary as the current approach is not applicable to non-isolated crossings occurring at short internuclear distances.**

Experimental results

The yield of neutral pairs as a function of the separation r between the products for the three acquired data sets (see Table I) are shown in Fig. 3(a), 3(b), and 3(c) respectively. As different beam energies and collision energies were used for the different data sets, the measured separations then correspond to different final kinetic energies (see equation 2) as highlighted in the top scales of the figures, and hence different final states (equation 3 and 4)

For the first spectrum, Fig. 3(a), at 0.07 ± 0.01 eV collision energy, slower ion beams were used in order to resolve the channels resulting in iodine in the $6s \ ^2[2]$ excited state. Thus the separations correspond to kinetic energies only up to 3 eV. The two channels (equation 3), corresponding to the spin-orbit splitting of this excited state, can be clearly distinguished in the spectrum, with the $J=5/2$ state found to dominate. In the second data set, Fig. 3(b), a similar collision energy was achieved, namely 0.10 ± 0.02 eV. The same two peaks (from Fig. 3(a)) are then located at lower separations (around 1 cm), due to the higher beam energies used but are no longer resolved. However, a second peak appears at larger separations, corresponding to pairs of iodine atoms in the ground state configuration (equation 4). Since the broadening of the distributions scales with kinetic energy, the individual J -state pairs are not resolved, but the width of the peak indicates that contributions from all three channels are present.

The observed rate for this measurement was found to be commensurate to the O^+/O^- collision system previously studied at DESIREE[28], for which the cross section is well known[27]. We therefore estimate the cross section to be in the range of 10^{-13} cm² (± 1 order of magnitude) at this collision energy (~ 0.1 eV).

In the third measurement, Fig. 3(c), the same beam energies as in Fig. 3(b) were used, but the drift-tubes were biased to yield a slightly higher collision energy, i.e. 0.80 ± 0.10 eV. This results in a lower count rate, due to the expected $1/E_{c.m.}$ cross section dependence on the collision energy, as well as additional broadening and a shift in the separations. However, the two main peaks are still fully resolved and within the detectable range.

For the three spectra, the result from the fits of the simulated distributions are shown as full black lines, with the individual distributions shown in colored lines: blue for the excited/ground state pairs and red for the different ground state configuration pairs. While the peaks are found to become broader as the collision energy increases, the relative intensities appear to be mostly unchanged. In addition, two small features appear to not correspond to any of the channels: One at short separations, below the lower energetic channels, is believed to be an artifact of the background model used. **The second one, around 1.5 eV, is likely to be a contribution from the first fine-structure state of the cation, namely $I^+(^3P_0)$. Since the state is about 0.8 eV above the ground state, it can be expected to be populated to some degree when produced in an ECR source. The observed peak positions (marked with an asterisk in the spectra) are found to correspond to the channels of equation 3 with this additional energy. In the higher collision energy measurement 3(c), the peak is not observed as it cannot be resolved from the main peak.** Storage of up to 20 seconds did not reveal any change in the signal, suggesting that the latter lives for a longer time. This can be explained by the necessity of a quadrupole transition ($\Delta J = 2$) for decay to the ground state.

Based on the fits, the branching ratios were extracted, with the lower collision energy measurement ($E_{c.m.} \sim 0.07$ eV) used to determine the relative intensity of the two excited channels at 0.1 eV collision energy. This is motivated as the branching ratios are not expected to change drastically over such a small range of collision energies. The results are presented in Fig. 4 with the full details presented in Table II.

All energetically open channels are found to be populated to some extent, with the $^2[2]_{5/2} + ^2P_{3/2}^{\circ}$ channel found to dominate at the measured collision energies. For the ground state configuration pairs, the $^2P_{1/2}^{\circ} + ^2P_{3/2}^{\circ}$ is favoured, while a lower population is observed for the $J=1/2$ pair compared to the $J=3/2$ pair. As the individual channels are not fully resolved, the branching ratios have rather large uncertainties, as indicated by the error bars. **The two main peaks are, however, clearly separated and thus their total branching ratios can be determined directly by evaluating the area under**

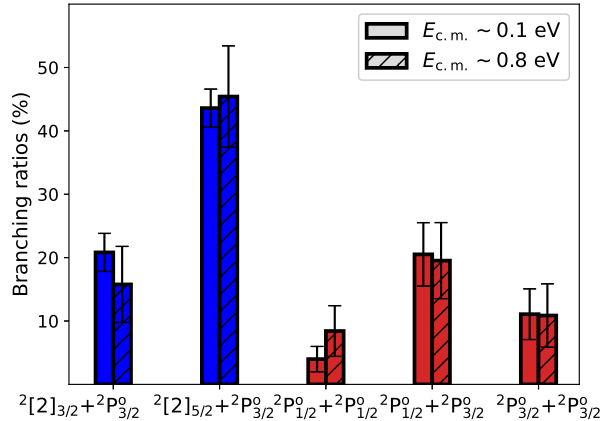


FIG. 4. Branching ratios of the mutual neutralization of I^+ with I^- at the two measured collision energies.

TABLE II. Experimental branching ratios of the different channels at the collision energy of 0.1 and 0.8 eV.

Product channel	E_K (eV)	Exp 0.1 eV	Exp 0.8 eV
$^2[2]_{3/2} + ^2P_{3/2}^o$	0.44	$21 \pm 3\%$	$16 \pm 6\%$
$^2[2]_{5/2} + ^2P_{3/2}^o$	0.62	$44 \pm 3\%$	$45 \pm 8\%$
$^2P_{1/2}^o + ^2P_{1/2}^o$	5.51	$4 \pm 2\%$	$8 \pm 4\%$
$^2P_{1/2}^o + ^2P_{3/2}^o$	6.45	$20 \pm 5\%$	$20 \pm 6\%$
$^2P_{3/2}^o + ^2P_{3/2}^o$	7.39	$11 \pm 4\%$	$11 \pm 5\%$
$^2[2] + ^2P^o$	~ 0.5 eV	$65 \pm 1\%$	$61 \pm 3\%$
$^2P^o + ^2P^o$	~ 6.5 eV	$35 \pm 1\%$	$39 \pm 3\%$

the respective peaks. The uncertainties are then given by the counting statistics and the error in the background. These smaller errors are shown in the last two rows of the table. The results show that the branching ratios do not differ significantly for the two energies considered.

IV. SUMMARY

In this work, we have studied the mutual neutralization of I^+ with I^- , using *ab initio* relativistic electronic structure calculations and merged beam techniques at the double electrostatic ion beam storage ring DESIREE. We have measured the branching ratios for the different channels using product-imaging methods combining position and timing information. Our results show that the reaction either forms high-kinetic-energy iodine neutral pairs in the ground state configuration or slow neutral pairs with one iodine atom in the $6s^2[2]$ excited state, through avoided crossings at short internuclear distances. Experimentally, these two channels were found to have a population of about 40%/60%, with no significant dependence on the collision energy in the studied range (0.1-

0.8eV), and with an observed rate commensurate with a previously studied system[28] (cross section of $\sim 10^{-13}$ cm² at 0.1 eV collision energy). These results are relevant to the modeling and diagnostics of low temperature iodine plasmas [31], which are promising candidates as propellants for electric space propulsion. Data on recombination processes are essential to model these plasmas, as these reactions can have substantial effects on the efficiency and ignition time of the engines [32]. Furthermore, the atoms formed after MN can undergo further reactions. For example, in [6] and [10] the authors consider atomic iodine excitation and ionization by electron impact as well as surface recombination. However, they used data that were obtained for iodine in the ground electronic state. The cross sections of these reactions are expected to be different for electronic excited states of iodine. Knowledge of the final state distribution of MN reaction, as provided in the present study, is therefore essential to obtain a more accurate description of iodine plasmas. The results discussed here will be combined with theoretical calculations in order to develop and improve the accuracy in modeling mutual neutralization reactions involving iodine species, efforts which will be extended to include more complex reactions involving molecular ions.

V. ACKNOWLEDGEMENTS

XY and ASPG acknowledge funding from projects Labex CaPPA (ANR-11-LABX-0005-01) and ComPRIXS (ANR-19-CE29-0019, DFG JA 2329/6-1), the I-SITE ULNE project OVERSEE and MESONM International Associated Laboratory (LAI) (ANR-16-IDEX-0004), and support from the French national supercomputing facilities (grant DARI A0090801859). This work was performed at the Swedish National Infrastructure, DESIREE (Swedish Research Council Contracts No. 2017-00621 and 2021-00155), and the authors thank the staff of DESIREE for their crucial contributions. The work is part of the project "Probing charge- and mass-transfer reactions on the atomic level", supported by the Knut and Alice Wallenberg Foundation (2018.0028), and is based upon work from COST Action (CA18212) - Molecular Dynamics in the GAS phase (MD-GAS), supported by COST (European Cooperation in Science and Technology). HTS and HZ acknowledge funding from the Swedish Research Council (contract Nos 2018-04092, 2020-03437). This material is based upon work supported by the Air Force Office of Scientific Research under Award No. FA9550-19-1-7012 (R.D.T.). The authors thank Alice Schmidt-May for analysis code development. NS thanks Anne Bourdon, Jean-Paul Booth for fruitful discussions, and Plas@par for financial support.

VI. APPENDIX

Table III lists the five lowest dissociation limits of I_2 . When considering spin-orbital coupling, there are three valence channels for $I(5p^5) + I(5p^5)$: ${}^2P_{3/2}^\circ + {}^2P_{3/2}^\circ$, ${}^2P_{1/2}^\circ + {}^2P_{3/2}^\circ$, ${}^2P_{1/2}^\circ + {}^2P_{1/2}^\circ$ as well as two Rydberg channels for $I(5p^46s^1) + I(5p^5)$: ${}^2[2]_{5/2} + {}^2P_{3/2}^\circ$ and ${}^2[2]_{3/2} + {}^2P_{3/2}^\circ$. The corresponding energy gaps of the ${}^2P_{3/2}^\circ - {}^2P_{1/2}^\circ$ and ${}^2[2]_{5/2} - {}^2P_{3/2}^\circ$ are 1.0 eV and 6.63 eV, which are in reasonable agreement with experimental value of 0.94 eV and 6.77 eV, respectively. On the other hand, for the separation of the 6s Rydberg state ${}^2[2]_{3/2} - {}^2[2]_{5/2}$, the computed value 0.62 eV is higher than the available experimental value of 0.18 eV.

A. Valence states

There are a total of 22 valence states corresponding to the lowest three dissociation limits, and as it can be seen from Figure 2, most of the molecular states are either repulsive states or quasi-bound states except for four states: $X\ 0_g^+$, $A\ 2_u$, $A\ 1_u$ and $B\ 0_u^+$, which are consistent with experimental results. The spectroscopic constants of these four states including equilibrium distance R_e , adiabatic excitation energy T_e , and vibrational constant ω_e are compared to experimental data and recently complete active space with second order perturbation theory correction (CASPT2) results in Table IV. It can be seen from the table that our calculations predict T_e rather well, showing average errors no larger than 200 cm^{-1} . For the equilibrium distance, the difference between MRCI and the experimental value is nearly identical with those of CASPT2.

Apart from these valence excited states, we also observe several Rydberg states at energies around 56000, 61000 and 67000 cm^{-1} . We note the R_e of such Rydberg states are around 2.66 Å, that is close to the R_e of ground state $X^2\Pi_{3/2g}$ of I_2^+ [33]. So they may belong to a Rydberg series, which converge on the ionization energy threshold associated with the ground state of I_2^+ .

B. Ion-Pair states

The ion-pair states exhibit dominantly a repulsive Coulomb character. We also fit the corresponding spectroscopic constants of the bound states by LEVEL according to the PECs. The result of T_e and R_e are then collected in Table V for comparison.

The total of 18 IPr states correspond to four different atomic states of I^+ : 3P_2 , 3P_1 , 3P_0 , and 1D_2 . There is a systematic difference for R_e . The computed R_e values are larger than the experimental ones by about 0.1 Å. For the adiabatic excitation energy, the deviations for most states are about 1000 cm^{-1} . Our computations also reproduce a pattern indicated in CASPT2 calculation [34], that is,

the difference of R_e between gerade states are smaller than that of the ungerade states.

C. Background subtraction

The experimental distributions prior to background subtraction are shown in Figure 5. This signal corresponds to the data for which the center-of-mass of the two particles are within a 5 mm radius, and contains both MN events and background. Outside this radius, the signal should only contain background. Assuming the center-of-mass distribution of the background is random, this signal may be used as a model for the background. An initial fit was therefore made with this model, which is shown as a gray line in the figure. This background model was then subtracted to yield the background-corrected spectra presented in Figure 3.

TABLE III. Dissociation relationships of I_2 . The molecular state is identified by the projection of total electronic angular momentum(Ω). **The number of states for each symmetry of Ω state** is given in the parenthesis.

Dissociation limits	Molecular states	Energy level (eV)	
		MRCI (this work)	Exp [35]
${}^2P_{3/2}^\circ + {}^2P_{3/2}^\circ$	$2_g(1), 1_g(1), 0_g(2), 2_u(1), 1_u(2), 0_u(2)$	0	0
${}^2P_{1/2}^\circ + {}^2P_{3/2}^\circ$	$2_g(1), 1_g(2), 0_g(2), 2_u(1), 1_u(2), 0_u(2)$	1.04	0.943
${}^2P_{1/2}^\circ + {}^2P_{1/2}^\circ$	$0_g(1), 1_u(1), 0_u(1)$	1.99	1.885
${}^2[2]_{5/2} + {}^2P_{3/2}^\circ$	$2_g(3), 1_g(4), 0_g(4), 2_u(3), 1_u(4), 0_u(4)$	6.629	6.774
${}^2[2]_{3/2} + {}^2P_{3/2}^\circ$	$2_g(2), 1_g(3), 0_g(4), 2_u(2), 1_u(3), 0_u(4)$	7.248	6.954

TABLE IV. Spectroscopic constants of the lowest four bound Ω states of I_2 .

State	$T_e(\text{cm}^{-1})$	$R_e(\text{\AA})$	$\omega_e(\text{cm}^{-1})$	Method
X 0_g^+	0	2.717	236.4	MRCI (this work)
	0	2.651	215.9	CASPT2 [34]
	0	2.666	214.5	Exp. [36]
A 2_u	10119	3.124	117.7	MRCI (this work)
		3.014	124.0	CASPT2 [34]
	10042	3.073	108.3	Exp. [36]
A 1_u	11162	3.173	92.0	MRCI (this work)
		3.040	114.6	CASPT2 [34]
	10907	3.114	93.0	Exp. [36]
B 0_u^+	15915	3.089	112.6	MRCI (this work)
		2.991	135.3	CASPT2 [34]
	15769	3.025	125.7	Exp. [36]

TABLE V. Spectroscopic constants of the ion-pair states of I_2 . Experimental values (taken from [36] and references therein) are given in parenthesis.

State	$T_e(\text{cm}^{-1})$	$R_e(\text{\AA})$	Dissociation limits
D' 2_g	40764 (40388)	3.712 (3.594)	${}^3P_2 + {}^1S_0$
$\beta 1_g$	41438 (40821)	3.721 (3.607)	${}^3P_2 + {}^1S_0$
D 0_u^+	42314 (41026)	3.737 (3.584)	${}^3P_2 + {}^1S_0$
E 0_g^+	42499 (41411)	3.773 (3.647)	${}^3P_2 + {}^1S_0$
$\gamma 1_u$	42315 (41621)	3.814 (3.683)	${}^3P_2 + {}^1S_0$
$\delta 2_u$	42162 (41787)	3.900 (3.787)	${}^3P_2 + {}^1S_0$
f 0_g^+	47971 (47026)	3.692 (3.574)	${}^3P_0 + {}^1S_0$
g 0_g^-	48717 (47086)	3.672 (3.572)	${}^3P_1 + {}^1S_0$
F 0_u^+	48961 (47217)	3.712 (3.600)	${}^3P_0 + {}^1S_0$
G 1_g	48694 (47559)	3.654 (3.549)	${}^3P_1 + {}^1S_0$
H 1_u	49327 (48280)	3.749 (3.653)	${}^3P_1 + {}^1S_0$
h 0_u^-	49467 (48646)	3.899 (3.780)	${}^3P_1 + {}^1S_0$
F' 0_u^+	54363 (51706)	3.557 (3.479)	${}^1D_2 + {}^1S_0$
1_g	55934 (53216)	3.623 (3.522)	${}^1D_2 + {}^1S_0$
f' 0_g^+	58306 (55409)	3.963 (3.825)	${}^1D_2 + {}^1S_0$

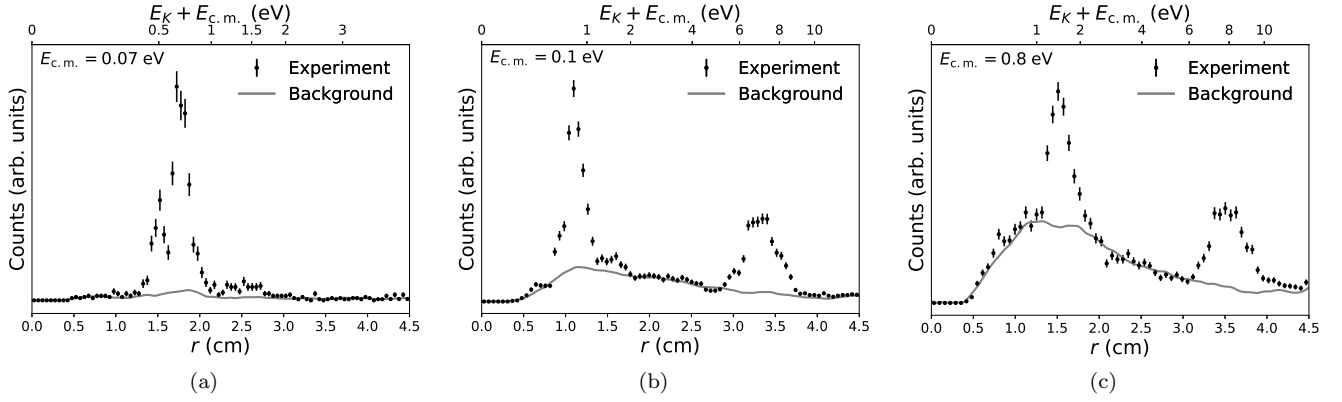


FIG. 5. Spectra of Fig. 3 prior to background subtraction. The background model, which is based on the excluded events in the data analysis, as described in Appendix C, was fitted to the data and is shown here as a full grey line.

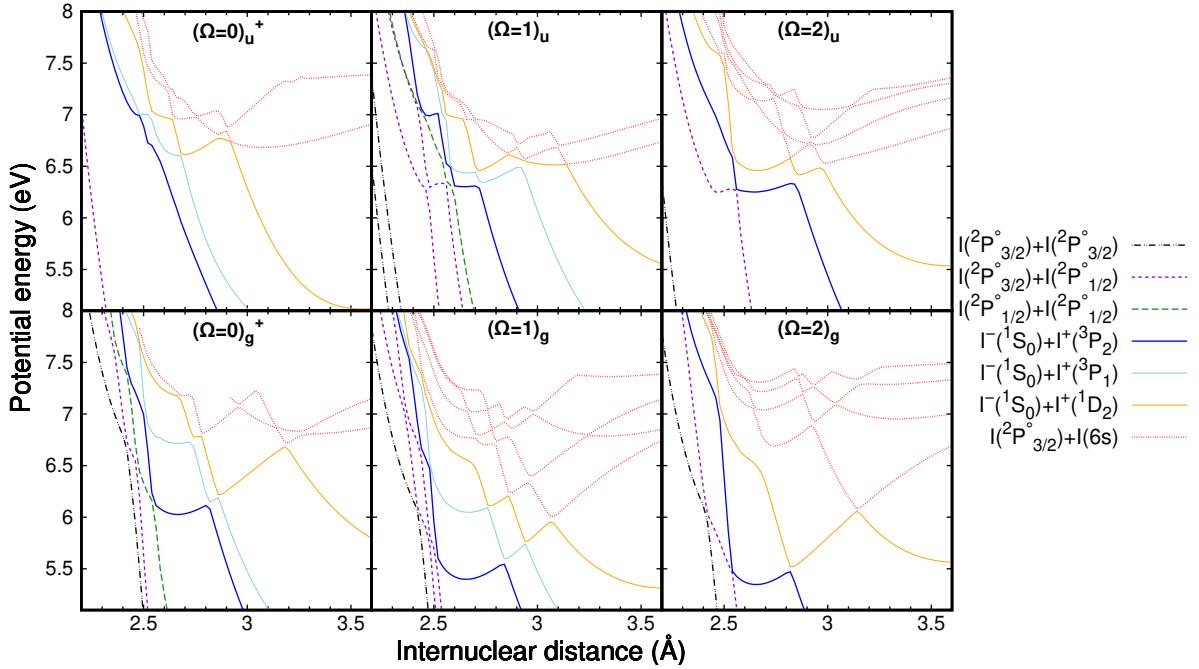


FIG. 6. Detailed view of the MRCI PECs of the electronic states of I_2 at short internuclear distances. Note that the energy for the highest state of symmetry 0_g^+ could not be computed below 2.9 \AA within the implementation of our method, as seen in the lowest left panel.

- [1] S. Mazouffre, *Plasma Sources Sci. Technol.* **25**, 033002 (2016), <https://doi.org/10.1088/0963-0252/25/3/033002>.
- [2] I. Levchenko, S. Xu, G. Teel, D. Mariotti, M. L. R. Walker, and M. Keidar, *Nature Communications* **9**, 879 (2018), <https://doi.org/10.1038/s41467-017-02269-7>.
- [3] E. Y. Choueiri, *J. Propuls. Power* **20**, 193 (2004), <https://doi.org/10.2514/1.9245>.
- [4] R. Lucken, *Theory and simulation of low-pressure plasma transport phenomena : Application to the PEGASES Thruster*, Ph.D. thesis, Université Paris Saclay (COMUE) (2019).
- [5] V. Croes, A. Tavant, R. Lucken, R. Martorelli, T. Lafleur, A. Bourdon, and P. Chabert, *Physics of Plasmas* **25**, 063522 (2018), <https://doi.org/10.1063/1.5033492>.
- [6] P. Grondein, T. Lafleur, P. Chabert, and A. Aanesland, *Physics of Plasmas* **23**, 033514 (2016), <https://doi.org/10.1063/1.4944882>.
- [7] K. Holste, W. Gärtner, D. Zschätzsch, S. Scharmann, P. Köhler, P. Dietz, and P. J. Klar, *Eur. Phys. J. D* **72**, 9 (2018), <https://doi.org/10.1140/epjd/e2017-80498-5>.
- [8] B. D. Prince, D. J. Levandier, and R. J. Bemish, in *53rd AIAA/SAE/ASEE Joint Propulsion Conference*, <https://doi.org/10.2514/6.2017-4634>.
- [9] P. Dietz, W. Gärtner, Q. Koch, P. E. Köhler, Y. Teng, P. R. Schreiner, K. Holste, and P. J. Klar, *Plasma Sources Sci. Technol.* **28**, 084001 (2019), <https://doi.org/10.1088/1361-6595/ab2c6c>.
- [10] D. Levko and L. L. Raja, *Journal of Applied Physics* **130**, 173302 (2021), <https://doi.org/10.1063/5.0063578>.
- [11] T. H. Y. Yeung, *Proceedings of the Physical Society* **71**, 341 (1958).
- [12] A. S. P. Gomes, T. Saue, L. Visscher, H. J. A. Jensen, R. Bast, I. A. Aucar, V. Bakken, K. G. Dyall, S. Dubillard, U. Ekström, E. Eliav, T. Enevoldsen, E. Faßhauer, T. Fleig, O. Fossgaard, L. Halbert, E. D. Hedegård, T. Helgaker, B. Helmich-Paris, and S. Yamamoto, DIRAC19 (v19.0). Zenodo, <https://doi.org/10.5281/zenodo.3572669>.
- [13] T. Saue, R. Bast, A. S. P. Gomes, H. J. A. Jensen, L. Visscher, I. A. Aucar, R. Di Remigio, K. G. Dyall, E. Eliav, E. Fasshauer, T. Fleig, L. Halbert, E. D. Hedegård, B. Helmich-Paris, M. Iliáš, C. R. Jacob, S. Knecht, J. K. Laerdahl, M. L. Vidal, M. K. Nayak, M. Olejniczak, J. M. H. Olsen, M. Pernpointner, B. Senjean, A. Shee, A. Sunaga, and J. N. P. van Stralen, *J. Chem. Phys.* **152**, 204104 (2020), <https://doi.org/10.1063/5.0004844>.
- [14] K. G. Dyall, *Theor. Chem. Acc.* **115**, 441 (2006), <https://doi.org/10.1007/s00214-006-0126-0>.
- [15] T. Fleig, J. Olsen, and L. Visscher, *J. Chem. Phys.* **119**, 2963 (2003), <https://doi.org/10.1063/1.1590636>.
- [16] R. J. Le Roy, *J. Quant. Spectrosc. Radiat. Transf.* **186**, 167 (2017), <https://doi.org/10.1016/j.jqsrt.2016.05.028>.
- [17] R. D. Thomas, H. T. Schmidt, G. Andler, M. Björkhage, M. Blom, L. Brännholm, E. Bäckström, H. Danared, S. Das, N. Haag, P. Halldén, F. Hellberg, A. I. S. Holm, H. A. B. Johansson, A. Källberg, G. Källersjö, M. Larsson, S. Leontin, L. Liljeby, P. Löfgren, B. Malm, S. Mannervik, M. Masuda, D. Misra, A. Orbán, A. Paál, P. Reinhed, K.-G. Rensfelt, S. Rosén, K. Schmidt, F. Seitz, A. Simonsson, J. Weimer, H. Zettergren, and H. Cederquist, *Rev. Sci. Instrum.* **82**, 065112 (2011), <https://doi.org/10.1063/1.3602928>.
- [18] H. T. Schmidt, R. D. Thomas, M. Gatchell, S. Rosén, P. Reinhed, P. Löfgren, L. Brännholm, M. Blom, M. Björkhage, E. Bäckström, J. D. Alexander, S. Leontin, D. Hanstorp, H. Zettergren, L. Liljeby, A. Källberg, A. Simonsson, F. Hellberg, S. Mannervik, M. Larsson, W. D. Geppert, K. G. Rensfelt, H. Danared, A. Paál, M. Masuda, P. Halldén, G. Andler, M. H. Stockett, T. Chen, G. Källersjö, J. Weimer, K. Hansen, H. Hartman, and H. Cederquist, *Rev. Sci. Instrum.* **84**, 055115 (2013), <https://doi.org/10.1063/1.4807702>.
- [19] G. Eklund, J. Grumer, S. Rosén, M. Ji, N. Punnakayathil, A. Källberg, A. Simonsson, R. D. Thomas, M. H. Stockett, P. Reinhed, P. Löfgren, M. Björkhage, M. Blom, P. S. Barklem, H. Cederquist, H. Zettergren, and H. T. Schmidt, *Phys. Rev. A* **102**, 012823 (2020).
- [20] S. Rosén, H. T. Schmidt, P. Reinhed, D. Fischer, R. D. Thomas, H. Cederquist, L. Liljeby, L. Bagge, S. Leontin, and M. Blom, *Rev. Sci. Instrum.* **78**, 113301 (2007), <https://doi.org/10.1063/1.2814030>.
- [21] Z. Amitay and D. Zajfman, *Rev. Sci. Instrum.* **68**, 1387 (1997), <https://doi.org/10.1063/1.1147950>.
- [22] D. Zajfman, Z. Amitay, M. Lange, U. Hechtfisher, L. Knoll, D. Schwalm, R. Wester, A. Wolf, and X. Urbain, *Phys. Rev. Lett.* **79**, 1829 (1997), <https://doi.org/10.1103/PhysRevLett.79.1829>.
- [23] Z. Amitay, A. Baer, M. Dahan, J. Levin, Z. Vager, D. Zajfman, L. Knoll, M. Lange, D. Schwalm, R. Wester, A. Wolf, I. F. Schneider, and A. Suzor-Weiner, *Phys. Rev. A* **60**, 3769 (1999), <https://doi.org/10.1103/PhysRevA.60.3769>.
- [24] R. D. Thomas, *Mass Spectrom. Rev.* **27**, 485 (2008), <https://doi.org/10.1002/mas.20169>.
- [25] T. Launoy, J. Loreau, A. Dochain, J. Liévin, N. Vaeck, and X. Urbain, *ApJ* **883**, 85 (2019), <https://doi.org/10.3847/1538-4357/ab3346>.
- [26] J. Grumer, G. Eklund, A. M. Amarsi, P. S. Barklem, S. Rosén, M. Ji, A. Simonsson, H. Cederquist, H. Zettergren, and H. T. Schmidt, *Phys. Rev. Lett.* **128**, 033401 (2022), <https://doi.org/10.1103/PhysRevLett.128.033401>.
- [27] N. de Ruelle, A. Dochain, T. Launoy, R. F. Nascimento, M. Kaminska, M. H. Stockett, N. Vaeck, H. T. Schmidt, H. Cederquist, and X. Urbain, *Phys. Rev. Lett.* **121**, 083401 (2018), <https://doi.org/10.1103/PhysRevLett.121.083401>.
- [28] M. Poline, A. Dochain, S. Rosén, J. Grumer, M. Ji, G. Eklund, A. Simonsson, P. Reinhed, M. Blom, N. S. Shuman, S. G. Ard, A. A. Viggiano, M. Larsson, H. Cederquist, H. T. Schmidt, H. Zettergren, X. Urbain, P. S. Barklem, and R. D. Thomas, *Phys. Chem. Chem. Phys.* **23**, 24607 (2021), <https://doi.org/10.1039/D1CP03977F>.
- [29] G. Eklund, J. Grumer, P. S. Barklem, S. Rosén, M. Ji, A. Simonsson, R. D. Thomas, H. Cederquist, H. Zettergren, and H. T. Schmidt, *Phys. Rev. A* **103**, 032814 (2021), <https://doi.org/10.1103/PhysRevA.103.032814>.
- [30] R. E. Olson, J. R. Peterson, and J. Moseley, *J. Chem. Phys.* **53**, 3391 (1970), <https://doi.org/10.1063/1.1674506>.

- [31] L. L. Alves, A. Bogaerts, V. Guerra, and M. M. Turner, *Plasma Sources Sci. Technol.* **27**, 023002 (2018), <https://doi.org/10.1088/1361-6595/aaa86d>.
- [32] S. Williams, A. Midey, S. Arnold, P. Bench, A. A. Viggiano, R. Morris, L. Maurice, and C. Carter, in *9th International Space Planes and Hypersonic Systems and Technologies Conference*, <https://doi.org/10.2514/6.1999-4907>.
- [33] L.-h. Deng, Y.-y. Zhu, C.-l. Li, and Y.-q. Chen, *J. Chem. Phys.* **137**, 054308 (2012), <https://doi.org/10.1063/1.4739466>.
- [34] V. A. Alekseev, *Opt. Spectrosc.* **116**, 329 (2014), <https://doi.org/10.1134/S0030400X14030023>.
- [35] A. Kramida, Yu. Ralchenko, J. Reader, and NIST ASD Team, NIST Atomic Spectra Database (version 5.9), [Online] National Institute of Standards and Technology, Gaithersburg, MD. (2021), <https://dx.doi.org/10.18434/T4W30F>.
- [36] S. Lukashov, A. Petrov, and A. Pravilov, *The Iodine Molecule* (Springer International Publishing, Cham, 2018) <https://doi.org/10.1007/978-3-319-70072-4>.